THE CONDUCTED ACTION POTENTIAL

Models and Comparison to Experiments

MARC K. WALTON AND HARRY A. FOZZARD
Departments of The Pharmacological and Physiological Sciences and of Medicine, The University of Chicago, Chicago, Illinois 60637

ABSTRACT Propagation of the action potential is a complex process, and the relationships among the various factors involved in conduction have not been clear. We use three mathematical models of uniform conduction in a cable to clarify some of these relationships. One model is newly derived here, and two have been previously derived by Hunter et al. (1975, *Prog. Biophys. Mol. Biol.*, 30:99–144). These models were able to simulate individual experimental action potential upstrokes previously obtained (Walton and Fozzard, 1983, *Biophys. J.*, 44:1–8). The models were then utilized to provide relationships between measures of conduction. Among these were that maximal upstroke velocity ($\dot{V}_{max}$) is directly proportional to peak inward ionic current normalized by capacitance that is filled during the upstroke ($\hat{I}/C_f$), and that conduction velocity was directly related to the square root of either $\dot{V}_{max}$ or $\hat{I}/C_f$. These relationships were shown to be model independent and to predict the experimental results, thus providing validated quantitative relationships that were not discernible through use of experimental data alone. The concept of safety factor was considered and a parameter was proposed that may be related to safety factor.

INTRODUCTION

Models of propagation have long been utilized in efforts to understand the process of conduction of an action potential (e.g., Huxley, 1959; FitzHugh, 1969; Levin and Fozzard, 1981). The current concept of conduction is that the excitable membrane's active properties produce the ionic current that drives the conduction process in balance with the tissue's passive properties (Hodgkin and Huxley, 1952; Cooley and Dodge, 1966; Khodorov and Timin, 1975). This implies relationships between the active and passive properties that are not intuitively obvious, and models may be useful. In a companion study (Walton and Fozzard, 1983), some relationships between measures of conduction were examined experimentally, but the quantitative nature of the relationships was not clear from the experimental results. In this paper we examine three models for their value in providing insight into the relationships among parameters of conduction, and we validate some of these relationships by comparison with the experimental data.

We are concerned here with modeling the upstroke of the action potential. The goal is an understanding of conduction and its related currents that is not as readily obtainable with more complex models. The models presented here are descended directly from the work of Rushton (1937), and each utilizes the cable model. The outlines of the models are presented here, leaving the details to the Appendixes. Experimentally determinable values such as $\dot{V}_{max}$, θ, $\hat{I}$, etc. will be called upstroke properties, while values introduced in formulating the models will be identified as model parameters. In all these models, V is a relative potential; resting potential is defined as 0 mV, and the upstroke carries V positive to its peak, V_{pk}. To keep the models generalized to any tissue that can be considered a cable, the capacitor filled during the upstroke is represented here as C_f. (For a structure such as the squid giant axon, C_f is the same as the low frequency capacitance, C_m, while for cardiac Purkinje fibers it is not.)

The action potential will be treated as a sigmoidal upstroke curve (Fig. 1 *A*). This is a reasonable simplification because the peak height is maintained for some time compared with the upstroke's duration. The propagated upstroke will be isolated from the rest of the action potential because no axial current flows ($dV/dx = 0$). Each model begins with an assumed shape of the dV/dt curve ($\dot{V}$) and the assumption of the uniform cable. One model uses exponential forms for its basic assumption about $\dot{V}$, and is developed here for the first time (Appendix A). The other two models were derived by Hunter et al (1975), but not extensively compared by them with experimental data (HMN [Hunter-McNaughton-Noble] models). Their distinguishing feature is the use of a polynomial for the basic assumption about $\dot{V}$ (Appendixes B and C).

GLOSSARY

a	Radius of the cylindrically modeled fiber
C_m	Low frequency capacitance per unit cylindrical surface area
C_f	Capacitance filled during foot of upstroke; capacitance per unit cylindrical surface area

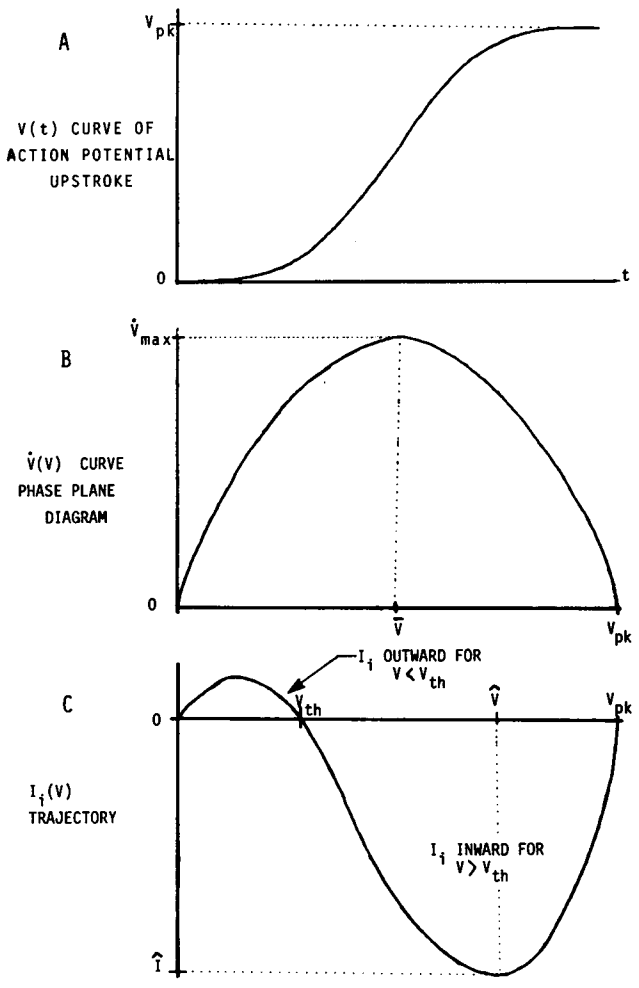

FIGURE 1 Idealized form of upstroke. (*A*) Membrane potential during upstroke, using relative membrane potentials where $V_r = 0$. (*B*) Idealized form of dV/dt ($\dot{V}$) plotted in phase plane format: $\dot{V}$ vs. V. (*C*) Ionic current also shown as a function of potential during the upstroke. This curve was drawn to show threshold phenomenon. This shape is similar to that used by HMN polynomial models.

- G Internal parameter of HMN models, scale factor for ionic current curve, conductance per unit area
- I_i Ionic current density across membrane ($\mu A/cm^2$ cylindrical surface area). Also refers to ionic current density during entire upstroke
- $\hat{I}$ Peak inward ionic current (I_i) during upstroke
- K Rate constant of rise of action potential foot, $(1/t)$
- P Power of ionic current during entire upstroke = $\int I_i dV$
- P_c Power of capacity current during entire upstroke = $\int I_c dV$
- R Ratio of K/β for exponential model
- R_i Specific resistivity of intracellular fluid (Ω – cm)
- R_m Specific membrane resistance (Ω – cm^2 cylindrical surface area)
- S Internal parameter for HMN models
- t Time
- U_c Energy change due to flow of capacity current during upstroke
- V Membrane potential (inside-outside) usually a relative potential where values are shifted so that resting potential is 0 mV
- $\bar{V}$ Potential at which $\dot{V}_{max}$ occurs
- V_{pk} Peak membrane potential, occurs at end of upstroke
- V_{th} Internal parameter of HMN models; potential at which I_i changes from outward to inward
- $\dot{V}$ dV/dt, especially as entire curve during upstroke
- $\dot{V}_{max}$ Maximum upstroke velocity; peak value of $\dot{V}$ during upstroke
- $\ddot{V}$ d^2V/dt^2; second derivative of voltage in time at one, fixed position
- α Internal parameter of exponential model
- β Internal parameter of exponential model; rate constant affecting decline in $\dot{V}$
- θ Conduction velocity (meters per second)
- ϕ_c Safety coefficient proposed in discussion, = $P_c U_c / C_f^2$
- $\Gamma(\ )$ Standard gamma function of mathematics, arises in development of exponential model (Appendix A).

EXPONENTIAL MODEL

This model begins by postulating the upstroke velocity curve ($\dot{V}$) as a function of time during the upstroke:

$$\dot{V}(t) = e^{Kt} \cdot e^{-\alpha e^{\beta t}}. \quad (1)$$

This is a function of an increasing exponential and a decreasing sigmoidal curve known as a Gompertz curve (Fig. 2). Gompertz curves have also been used by Easton

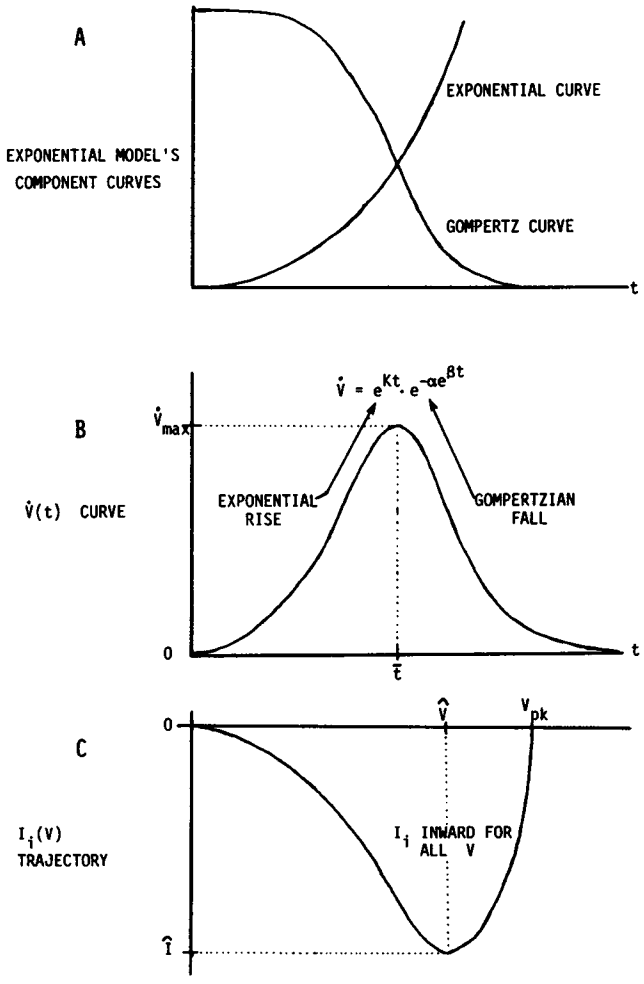

FIGURE 2 Exponential model of upstroke. (*A*) Exponentially rising curve and Gompertzian falling curve individually depicted. (*B*) $\dot{V}(t)$ curve of model. Rise due to domination of exponential portion of equation, fall due to domination of Gompertz portion of equation. (*C*) Resulting I_i trajectory is nonthreshold form.

(1978) to model the ionic conductance kinetics of voltage clamped nerve, producing a model with similar capabilities to the Hodgkin-Huxley model. The result here is a curve that is asymptotic to zero for $t \rightarrow \mp \infty$ and that has a transient rise (to $\dot{V}_{max}$) at some time positive to zero.

The model assumes the uniform cable relation with a uniformly conducted action potential is valid:

$$I_i = C_f(\ddot{V}/K - \dot{V}). \tag{2}$$

Combined, these produce a curve for I_i:

$$I_i(t) = -C_f(\alpha\beta/K)e^{(K+\beta)t-\alpha e^{\beta t}}. \tag{3}$$

This is a nonthreshold I_i curve (Fig. 2 *C*). An implied assumption in using this model is that for the phenomena of interest, the existence of a threshold for inward current is not important.

This model uses three parameters: K, β, and α. K is also the physiological rate constant of rise of the exponential foot of the action potential. This model has $\dot{V}(t) \sim e^{Kt}$ for early t when α is small, so that it is valid to use the rate constant of the upstroke foot in the model in this fashion, if we restrict α to be sufficiently small. α can be viewed as a unitless scale parameter to set the effect of a $1/\beta$ time constant on the gompertzian term. β is the rate constant of the gompertzian term, setting the rate at which the rise in $\dot{V}$ will decelerate and then decline to zero.

The experimental data reported in the companion article (Walton and Fozzard, 1983) consist of the passive cable properties (R_i, R_m, C_m) and the action-potential upstroke measurements. These are of two types: the single valued measures for K, θ, $\dot{V}_{max}$, V_{pk}, etc., and the continuous functions in time of $V(t)$, $\dot{V}(t)$, and $\ddot{V}(t)$ that were used to calculate a continuous curve for $I_i(t)$. Just as the continuous $\dot{V}(t)$ curve is more easily dealt with by its peak height and area ($\dot{V}_{max}$ and V_{pk}), the I_i curve is described by its peak height and area ($\hat{I}$ and $P = \int I_i dV$).

Values for such properties as $\dot{V}_{max}$, V_{pk}, $\hat{I}$, P may be calculated from the equations in Appendix A. The value for θ comes by use of the Tasaki-Hagiwara (1957) relation and the model's parameter K:

$$\theta = \frac{aK}{2R_iC_f}. \tag{4}$$

The values obtained from the experimentally measured upstrokes are those directly related to the velocity ($\dot{V}_{max}$, V_{pk}, K, $\bar{V}$, and θ) and those more related to the current ($\hat{I}$, P). The model was tested by using several of the measured values of upstroke properties from a single action-potential upstroke as input parameters to the model. The model was then used to calculate the other upstroke properties. These calculated values were then compared with the experimental values not used for input, to show how faithful the model is to the relationships between properties. This is a three-parameter model, so three independent constraints were needed. For the $\dot{V}$-related properties, the experimental values for $\dot{V}_{max}$, V_{pk}, and K were used to calculate a unique set of values for K, α, and β, which then generated a unique $\hat{I}$, P. However, for the I_i-related properties, only two experimental values are available, $\hat{I}$ and P. The necessary third constraint for this case was obtained by assigning a constant value for α for each experiment.

The significance of the model parameter K is clear, since it is also the upstroke property K, and it determines the initial rate of rise of the upstroke. The parameter β indicates slowing of membrane potential rise towards V_{pk}, a factor not usually dealt with in electrophysiological studies. However, just as K may be related to the development of the inward Na current, so may β be related to the decline of Na current. As V approaches its peak, inward Na current declines because of loss of driving force (which declines faster if V rises faster), and because of fall in Na permeability (which occurs sooner if V rises into the range of faster inactivation rate constants). β should be related to K, because faster rising upstrokes (K larger) will lead to faster loss of inward current, making β larger. If one makes the simple approximation $K/\beta = R$ a constant for each experiment, the number of variables is reduced.

Quantitative relationships between the various upstroke properties will be limited to $\dot{V}_{max}$, $\hat{I}$, K, and θ. $\hat{I}/C_f$ is used here rather than just $\hat{I}$ for the same reason as in the experimental study, the complex cross-sectional geometry of cardiac Purkinje strands. As developed in Appendix A, the relationships obtained are (using $R = K/\beta$) between K or θ and $\dot{V}_{max}$

$$K = \frac{e^R}{R^{R-1}}\Gamma(R)\frac{\dot{V}_{max}}{V_{pk}} \tag{5}$$

$$\theta = \sqrt{\frac{e^R}{2R^{R-1}}\Gamma(R)}\sqrt{\frac{a}{R_iC_f}}\sqrt{\frac{\dot{V}_{max}}{V_{pk}}} \tag{6}$$

between K or θ and $\hat{I}/C_f$

$$K = -R^2\left(\frac{e}{R+1}\right)^{R+1}\Gamma(R)\frac{\hat{I}/C_f}{V_{pk}} \tag{7}$$

$$\theta = \sqrt{R^2\left(\frac{e}{R+1}\right)^{R+1}\Gamma(R)}\sqrt{\frac{a}{2R_iC_f}}\sqrt{\frac{-\hat{I}/C_f}{V_{pk}}} \tag{8}$$

and between $\dot{V}_{max}$ and $\hat{I}/C_f$

$$\dot{V}_{max} = -e\left(\frac{R}{R+1}\right)^{R+1}\hat{I}/C_f. \tag{9}$$

HMN CUBIC MODEL

This model was developed by Hunter et al. (1975), and their formulation will be retained here (also see Appendix B). The model may also be started by postulating a form for the upstroke velocity curve, $\dot{V}$, but here the phase plane

representation [$\dot{V}$ as $f(V)$] is used:

$$\dot{V} = \frac{GS}{C_f} V\left(1 - \frac{V}{V_{pk}}\right). \tag{10}$$

This is a parabola (2° polynomial) starting at zero for $V = 0$, rising to $\dot{V}_{max}$, and falling back to zero at $V = V_{pk}$ (Fig. 1 *B*).

The cable equation is assumed valid, and Eqs. 2 and 10 are combined with a requirement for the I_i curve to display a threshold. I_i will be outward for small values of V, and inward (negative) after passing through $I_i = 0$ at some specific $V_{th} > 0$ (Fig. 1 *C*). The resulting cubic polynomial curve is

$$I_i = GV\left(1 - \frac{V}{V_{th}}\right)\left(1 - \frac{V}{V_{pk}}\right). \tag{11}$$

This model is also a three-parameter model. The parameters are G, V_{th}, and V_{pk}. G has units of conductance and scales the I_i curve to the appropriate height. V_{th} and V_{pk} set the zero current points for the model. Another factor, S, is not an independent parameter because it occurs in a fixed relationship to V_{th} and V_{pk}. Appendix B introduces $S > 0$ to insure a threshold, and then calculates V_{th} from S and V_{pk}:

$$V_{th} = (V_{pk}/2)\left(\frac{1}{S+1}\right). \tag{12}$$

Hence, S could be viewed as one of the three independent parameters of the model in place of V_{th} or V_{pk}, but this is not consistent with the original HMN development. In the HMN formulation, V_{th} was identified as representing the physiologic threshold for inward current, and S as a physiologic safety factor.

In this model K is not a parameter; it may be calculated from the others:

$$K = \frac{GS}{C_f}\left(\frac{S}{S+1}\right). \tag{13}$$

θ is found in the same way as before, calculated from K (Eq. 4).

Testing the model can be accomplished in a manner analogous to that for the exponential model. To use the $\dot{V}$-related properties, the experimental values for $\dot{V}_{max}$, V_{pk}, and K were applied, fixing the model parameters completely. In using the I_i-related properties only two experimental values are available, $\hat{I}$ and P. There are two ways to circumvent this problem, either to fix one of the model parameters as a third constraint or to add a third data value from the $\dot{V}$-related group. Four methods were tried. (*a*) A fixed G value was assigned for each fiber, and V_{th} and V_{pk} were allowed to vary to fit $\hat{I}$ and P. G was chosen from the midrange of G values obtained from the $\dot{V}$ data. (*b*) A G value was assigned for 100% Na solutions and G was allowed to decline proportionally to the fall in Na, because G is a scaling factor for I_i magnitude and the current should be proportional to Na. (*c*) A constant V_{th} value for each fiber was assigned, and G and V_{pk} were allowed to vary to fit $\hat{I}$ and P. The V_{th} value chosen was midrange for the values resulting from the $\dot{V}$-related calculations. (*d*) The experimental V_{pk} value was used as the third constraint.

This model's equations may also be recombined to obtain relations among the upstroke properties. As before, the internal parameters cannot be completely eliminated. S was introduced into the model to insure a threshold and had only the limit $S > 0$. Another way to view S is as a parameter indicating how close is the slope of the modeled upstroke $\dot{V}(V)$ foot to the experimental slope, K. A convenient way to eliminate S in the relations is to make S large, making the model's foot close to the experimental slope.

The relations obtained are between K or θ and $\dot{V}_{max}$

$$K = 4\frac{\dot{V}_{max}}{V_{pk}}\left(\frac{S}{S+1}\right) \tag{14}$$

$$\theta = \sqrt{\frac{2a}{R_i C_f}}\sqrt{\frac{\dot{V}_{max}}{V_{pk}}}\sqrt{\frac{S}{S+1}}; \tag{15}$$

between K or θ and $\hat{I}/C_f$

$$K = -\frac{27}{8}\frac{\hat{I}/C_f}{V_{pk}} \tag{16}$$

$$\theta = \sqrt{\frac{27a}{16R_i C_f}}\sqrt{\frac{-\hat{I}/C_f}{V_{pk}}} \quad \text{for large } S \tag{17}$$

and between $\dot{V}_{max}$ and $\hat{I}/C_f$

$$\dot{V}_{max} = -\frac{27}{32}\hat{I}/C_f \qquad \text{for large } S. \tag{18}$$

HMN QUINTIC MODEL

This model is much like the cubic model. It begins by assuming that a portion of a cubic describes the $\dot{V}(V)$ curve. It proceeds identically from there, resulting in

$$\dot{V}(V) = \frac{GS}{C_f} V\left(1 - \frac{V^2}{V_{pk}^2}\right) \tag{19}$$

$$I_i = GV\left(1 - \frac{V^2}{V_{th}^2}\right)\left(1 - \frac{V^2}{V_{pk}^2}\right). \tag{20}$$

Although the I_i curve is a quintic, it is not complete, having only three powers of V (V^1, V^3, V^5), so that it too is a three-parameter model. The parameters are G, V_{th}, V_{pk}. S occupies the same position as in the cubic model. This model is dealt with in all respects as the HMN cubic model. Between K or θ and $\dot{V}_{max}$

$$K = \frac{3\sqrt{3}}{2}\frac{\dot{V}_{max}}{V_{pk}}\left(\frac{S}{S+1}\right) \tag{21}$$

$$\theta = \sqrt{\frac{3\sqrt{3}}{4}\frac{a}{R_i C_f}}\sqrt{\frac{\dot{V}_{max}}{V_{pk}}}\sqrt{\frac{S}{S+1}}. \tag{22}$$

Between K or θ and $\hat{I}/C_f$

$$K = -\frac{25}{18}\sqrt{\frac{5}{3}}\frac{\hat{I}/C_f}{V_{pk}} \tag{23}$$

$$\theta = \sqrt{\frac{25\sqrt{15}}{108}}\frac{a}{R_i C_f}\sqrt{\frac{-\hat{I}/C_f}{V_{pk}}}. \quad \text{for large } S \tag{24}$$

Between $\dot{V}_{max}$ and $\hat{I}/C_f$

$$\dot{V}_{max} = -\frac{25}{81}\sqrt{5}\,\hat{I}/C_f. \quad \text{for large } S \tag{25}$$

Delayed activation models developed by Hunter et al. (1975) have additional complexities that make comparison with experimental data difficult or impossible. They cannot be conveniently compared with the models used here because of different types of assumptions, so they are not included.

RESULTS

Modeling of Individual Upstrokes

This section presents the results obtained when the models were used to simulate individual upstrokes of conducted action potentials (Walton and Fozzard, 1983). We first compared the experimental and the model-produced I_i curves with input of $\dot{V}$-related data, comparing for each curve the peak height, $\hat{I}$, and its area, P. When the I_i-related data were used as input for the model, a $\dot{V}$ curve was produced, and comparison was made with values for $\dot{V}_{max}$ (peak height of $\dot{V}$), V_{pk} (area under the $\dot{V}$ curve), and θ. Undue influence of one experiment on the magnitude of the results was eliminated by normalizing all results to the average of the values obtained in the 100% Na (control) solutions for each experiment. The resulting values for each parameter were plotted as modeled vs. experimental. An example is shown in Fig. 3; the HMN cubic model was used to model θ when $\hat{I}$, P, and V_{pk} were used as input parameters. The ideal result is for all points of all experiments to fall on a single straight line with a slope of 1.0. For Fig. 3, the correlation coefficient was 0.983 and the slope was 0.994, indicating that the model's variation in θ was very closely linked to the variation of θ in the data.

Each experimental upstroke was used to test the models, generating for each a correlation coefficient (r) and a slope (Table I). When $\dot{V}_{max}$, V_{pk}, and K were used for input in the HMN cubic model, good fits occurred for the changes in $\hat{I}$ and P. For the several methods of using $\hat{I}$ and P as input values, a range of results occurred. When the G parameter held constant, the results were fair for V_{pk} and $\dot{V}_{max}$, but

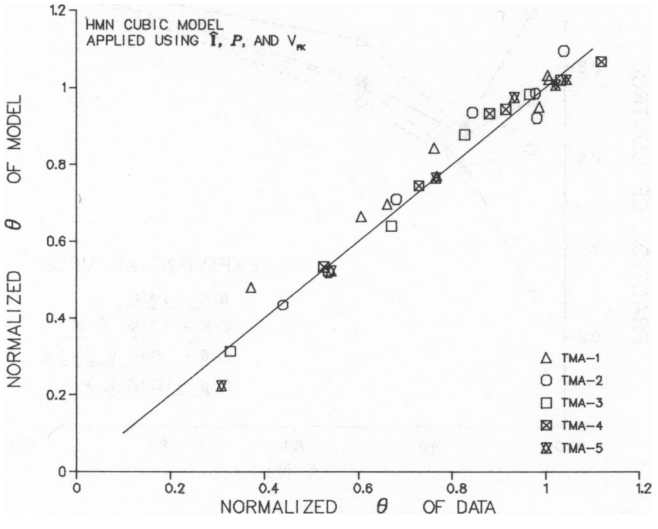

FIGURE 3 Comparison of conduction velocity (normalized to control) predicted by model with data value of conduction velocity. HMN cubic model used with $\hat{I}$, P, V_{pk} as input parameters. Straight line is ideal relationship of correlation coefficient = 1.0, slope = 1.0. Different symbols used for individual lowered Na experiments.

TABLE I
RESULTS OF TESTING MODELS ON INDIVIDUAL UPSTROKES

Model	$\hat{I}$	P	V_{pk}	$\dot{V}_{max}$	Θ	n
HMN cubic						
$\dot{V}_{max}$, V_{pk}, K input	0.955	0.998				
	0.846	1.01				
$\hat{I}$, P input						
G constant			0.812	0.938	0.367	30
			1.186	0.896	0.393	
G decreasing			0.881	0.936	0.178	31
			1.290	0.848	0.178	
V_{th} constant			0.940	0.996	0.984	31
			0.869	1.012	1.098	
V_{pk} input				0.999	0.983	31
				0.986	0.994	
HMN Quintic						
$\dot{V}_{max}$, V_{pk}, K input	0.957	0.997				21
	0.821	1.006				
$\hat{I}$, P input						
G constant			0.889	0.971	0.745	31
			1.134	0.917	0.627	
V_{th} constant			0.951	0.996	0.971	31
			1.034	0.975	0.937	
V_{pk} input				0.998	0.990	20
				0.988	1.003	
Exponential Model						
$\dot{V}_{max}$, V_{pk}, K input	0.830	0.998				31
	1.824	1.020				
	0.990	0.998				30
	0.994	1.019				
$\hat{I}$, P Input			0.889	0.987	0.914	31
			0.996	0.960	0.836	
			0.944	0.995	0.966	30
			0.910	0.989	0.952	

Comparison made between all values, normalized to control, for each parameter and for each appropriate method of applying models. Pairs of values shown are correlation coefficient (upper value) and slope of best-fit straight line for parameter values normalized by control of each experiment. Number of points model was able to provide simulations for given values, as n. For the exponential model, the results are shown with 1 outlying point omitted (n = 30).

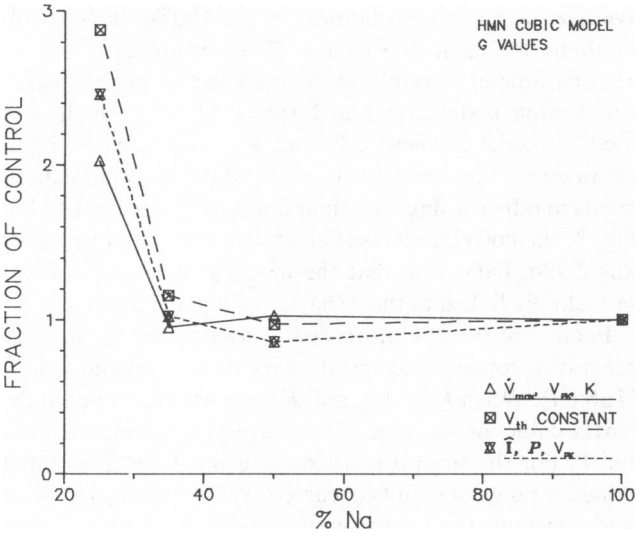

FIGURE 4 G parameter values from HMN cubic model. Points are of average, normalized to control, G values for each Na level. Method of applying model shown in key. Two methods of applying model not shown because G was used as input parameter (G constant, G decreasing).

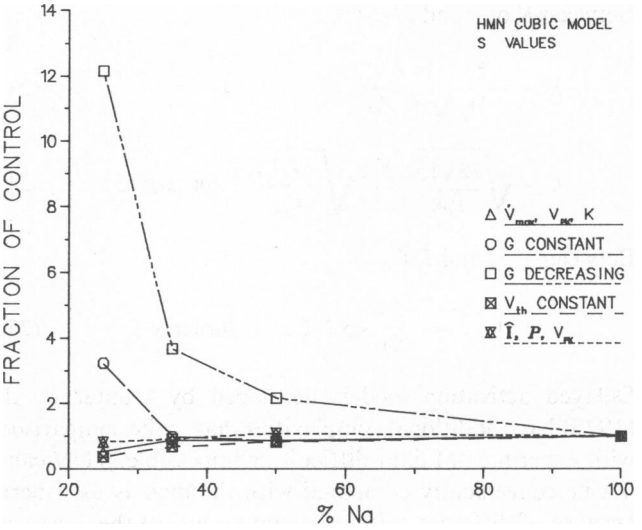

FIGURE 6 S values from HMN cubic model. Points are average, normalized to control, S values for each Na level with each method of applying model, identified in key.

poor for θ. When G was allowed to decline proportionally to the percent of Na, there was nearly no correlation. The reason for this can be seen from a graph of the average change in G if it was allowed to vary freely (Fig. 4). G remained constant for most solutions, but at 25% it showed a sharp rise. The forced decrease in G has even more difficulty, since it is contrary to the freely adjusted tendency in all cases. Better results were obtained for all three properties when G was allowed to vary and V_{th} was held constant. This was a reasonable expectation from the freely adjusted changes in V_{th} that occurred when $\dot{V}_{max}$, V_{pk}, and K were input values (Fig. 5). Using V_{pk} as a third parameter with $\hat{I}$ and P produced only marginally better results, since the fit was already good.

The HMN quintic model gave results slightly better than the cubic model for each method of application, with the hierarchy of accuracy retained. However, the quinic model was able to produce meaningful results for only 22 of the 31 upstrokes using the $\dot{V}$-related data, and for 21 of the upstrokes using the $\hat{I}$-related data. The failed-fit trials were distributed among all the experimental conditions, and the failures in one set did not match the failures in the

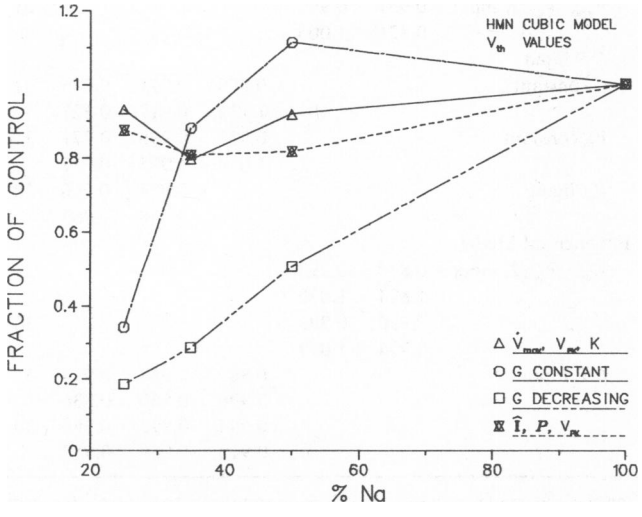

FIGURE 5 V_{th} values from HMN cubic model. Points are average, normalized to control, V_{th} values for each Na level with each method of applying model, identified in key. Method of constant V_{th} not shown because V_{th} acted as input parameter.

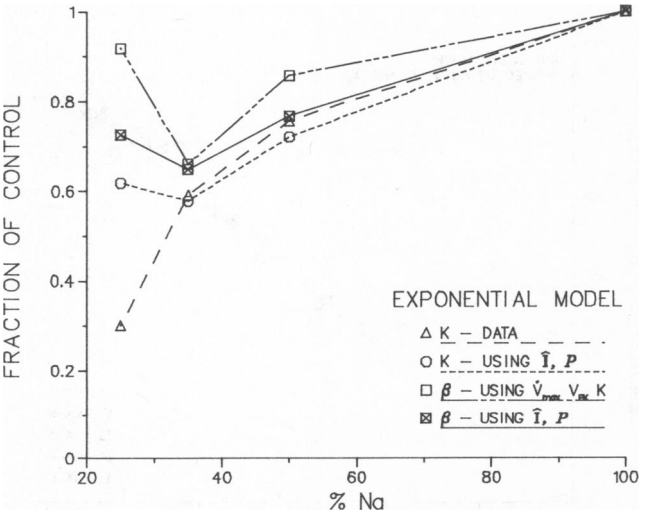

FIGURE 7 Average values of K and β from exponential model normalized by control. K and β shown for each method of applying model. Data value of K used in method of V_{max}, V_{pk}, K as input parameters. Deletion of 1 outlying point at 25% mostly acts to lower upper β curve and slightly raise lower K curve.

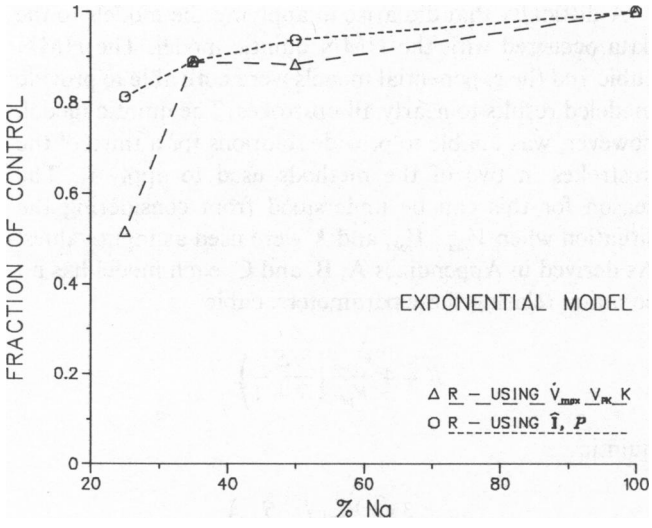

FIGURE 8 Average values of $R = K/\beta$ from exponential model, normalized to control. K of data used for R of $\dot{V}_{max}$, V_{pk}, K input method.

other set. While the fits with the quintic model could be very good, it was for a more restricted range of variation. The behavior of average changes in G and V_{th} are similar to those for the cubic model. The behavior of S in both the cubic and the qunitic models was inconsistent with an ideal safety factor. Only with constant V_{th} did the S values show the steady decline with reduced Na, although not to near zero. This is partly artifactual, since V_{pk} declines as Na falls so that S ($= V_{pk}/2V_{th} - 1$) is forced to decline if V_{th} is kept constant.

The results of the exponential model are also shown in Table I. It was able to fit all trials, although one trial consistently produced outliers. Table I shows correlations for both cases, with the outlying point included and with it excluded. Changes in K and β are shown in Fig. 7; both decline as Na falls. Changes in $R(K/\beta)$ are shown in Fig. 8. Particularly for the $\hat{I}$ and P input method, R fell very slowly.

Generalized Model Relationships

The relationships previously shown are collected into Tables II, III, and IV. They are shown without the simplifying assumptions, except in the case of HMN model relations involving $\hat{I}/C_f$, because a complex function of S is involved and they would only hide the relations of interest. Also shown are the slopes when the simplifying assumptions are applied.

K and θ are Proportional to $\dot{V}_{max}/V_{pk}$. In their simplified form, the relations between K and $\dot{V}_{max}$ are identical for all models, except for the slope (Table II). The specific slopes can be eliminated by normalization, and each model predicts the same thing: K is proportional to $\dot{V}_{max}/V_{pk}$ and is verified by the experimental data (Fig. 9). However, if we look at the nonnormalized predictions of the models (Fig. 10), it is apparent that the slope for the cubic model is not a good predictor of the experimental results. The HMN quintic model is a fairly good predictor of average behavior. The exponential model with the approximation of $R = 1$ is almost the same. The relationship between θ and $\dot{V}_{max}$ is the same, since θ has a fixed relation to K (Fig. 11).

$\hat{I}/C_f$ is proportional to $\dot{V}_{max}$. Table III shows the relations between $\dot{V}_{max}$ and $\hat{I}/C_f$. All three equations predict that normalized $\dot{V}_{max}$ and $\hat{I}/C_f$ will show a straight line relationship, and that was seen to correspond to the experimental data. When plotted without normalizing (Fig. 12), the data can be seen to form a fairly packed grouping about an average slope. The cubic model's line again lies higher than any of the data, while the HMN quintic model's line falls in about the middle of the grouping, again making it a better indicator of average behavior. The line for the exponential model with $R = 1$ also acts as a good approximation to the behavior of an average fiber. The remaining relations shown in Table IV

TABLE II
RELATION BETWEEN K OR Θ AND $\dot{V}_{max}$

	$K =$	$\Theta =$
HMN cubic	$4\frac{\dot{V}_{max}}{V_{pk}}\left(\frac{S}{S+1}\right)$	$\sqrt{2}\sqrt{\frac{a}{R_iC_f}}\sqrt{\frac{\dot{V}_{max}}{V_{pk}}}\left(\frac{S}{S+1}\right)^{1/2}$
HMN quintic	$\frac{3\sqrt{3}}{2}\frac{\dot{V}_{max}}{V_{pk}}\left(\frac{S}{S+1}\right)$	$\sqrt{\frac{3\sqrt{3}}{4}}\sqrt{\frac{a}{R_iC_f}}\sqrt{\frac{\dot{V}_{max}}{V_{pk}}}\left(\frac{S}{S+1}\right)^{1/2}$
Exponential	$R\left(\frac{e}{R}\right)^R \Gamma(R)\frac{\dot{V}_{max}}{V_{pk}}$	$\sqrt{\frac{R}{2}}\left(\frac{e}{R}\right)^{R/2}\Gamma(R)\sqrt{\frac{a}{R_iC_f}}\sqrt{\frac{\dot{V}_{max}}{V_{pk}}}$
Simplified form S large, HMN nonthreshold or R constant	$m\cdot\frac{\dot{V}_{max}}{V_{pk}}$	$m\cdot\sqrt{\frac{a}{R_iC_f}}\sqrt{\frac{\dot{V}_{max}}{V_{pk}}}$
Slopes (m)		
HMN cubic	4.0	1.4
HMN quintic	2.6	1.1
Exponential ($R = 1$)	2.7	1.2

TABLE III
RELATION BETWEEN $\dot{V}_{max}$ AND $\hat{I}/C_f$

HMN cubic (S large)	$\dot{V}_{max} = -\frac{27}{32}\hat{I}/C_f$
HMN quintic (S large)	$\dot{V}_{max} = -\frac{25}{81}\sqrt{5}\,\hat{I}/C_f$
Exponential	$\dot{V}_{max} = -e\left(\frac{R}{R+1}\right)^{R+1}\hat{I}/C_f$
Generalized S large, HMN nonthreshold or R constant	$\dot{V}_{max} = -m \cdot \hat{I}/C_f$
Slopes	
HMN cubic	0.84
HMN quintic	0.69
Exponential ($R = 1$)	0.68

involve K or θ and $\hat{I}/C_f$, and they are shown for completeness.

DISCUSSION

Simulation of Individual Upstrokes

It is clear that, although some methods of applying the models to individual upstrokes did not work well, when the models were applied with an appropriate method they were able to reproduce the changes seen in the experimental data. From this it must be concluded that the three models are able to simulate action potential upstrokes, at least as far as the characteristics important for determining these measured upstroke properties are concerned.

One aspect of these experiments that may have been important is the behavior of the action potential at its peak. These models all simulated a propagating action potential as just an upstroke with no repolarization phase. This is true in a Purkinje fiber action potential, but is probably not the case in squid axon (see for example, Jack et al., 1975, p. 282). In that case, it is V_{pk} that would be most subject to decrease due to repolarization. The HMN models utilize V_{pk} as an internal parameter, and so they might be more likely to have difficulties than the exponential model.

A difficulty that did arise in applying the models to the data occurred with the HMN quintic model. The HMN cubic and the exponential models were both able to provide modeled results to nearly all upstrokes. The quintic model, however, was unable to provide solutions for a third of the upstrokes in two of the methods used to apply it. The reason for this can be understood from considering the situation when $\dot{V}_{max}$, V_{pk}, and K were used as input values. As derived in Appendixes A, B, and C, each model has an equation relating these parameters: cubic

$$K = 4\frac{\dot{V}_{max}}{V_{pk}}\left(\frac{S}{S+1}\right),$$

quintic

$$K = \frac{3\sqrt{3}}{2}\frac{\dot{V}_{max}}{V_{pk}}\left(\frac{S}{S+1}\right),$$

and exponential

$$K = R\,(e/R)^R\,\Gamma(R)\,\frac{\dot{V}_{max}}{V_{pk}}.$$

The HMN models give an adjustable ratio of K to $\dot{V}_{max}/V_{pk}$, but with a maximum of 4 or 2.6 for the cubic or quintic models, respectively, when S is large. The cubic model can accommodate a much larger K for the same $\dot{V}_{max}/V_{pk}$ than can the quintic model. The exponential model is also highly adjustable, easily able to surpass the quintic model's limit (slope = 3.2 for R only 1.5) and encompass all the data utilized here. These relations were shown in Fig. 10 along with the data values. The cubic and exponential models can encompass all the data, but some results are beyond the capabilities of the quintic model.

A difference that was of little importance was that the HMN models were for ionic current trajectories with thresholds, while the exponential model was a nonthreshold type. Both were able to reproduce experimental changes well. A threshold in the ionic current is physiologi-

TABLE IV
RELATION BETWEEN K OR θ AND $\hat{I}/C_f$

HMN cubic	$K = -\frac{27}{8}\frac{\hat{I}/C_f}{V_{pk}}$	$\theta = \sqrt{\frac{27}{16}}\sqrt{\frac{a}{R_i C_f}}\sqrt{\frac{-\hat{I}/C_f}{V_{pk}}}$
HMN quintic	$K = -\frac{25}{18}\sqrt{\frac{5}{3}}\frac{\hat{I}/C_f}{V_{pk}}$	$\theta = \sqrt{\frac{25\sqrt{15}}{108}}\sqrt{\frac{a}{R_i C_f}}\sqrt{\frac{-\hat{I}/C_f}{V_{pk}}}$
Exponential	$K = -R^2\left(\frac{e}{R+1}\right)^{R+1}\Gamma(R)\frac{\hat{I}/C_f}{V_{pk}}$	$\theta = \frac{R}{\sqrt{2}}\left(\frac{e}{R+1}\right)^{R+1/2}\Gamma(R)^{1/2}\sqrt{\frac{a}{R_i C_f}}\sqrt{\frac{-\hat{I}/C_f}{V_{pk}}}$
Generalized S large, HMN nonthreshold or R constant	$K = -m \cdot \frac{\hat{I}/C_f}{V_{pk}}$	$\theta = m \cdot \sqrt{\frac{a}{R_i C_f}}\sqrt{\frac{-\hat{I}/C_f}{V_{pk}}}$
Slopes		
HMN cubic	3.4	1.3
HMN quintic	1.8	0.95
Exponential ($R = 1$)	1.8	0.96

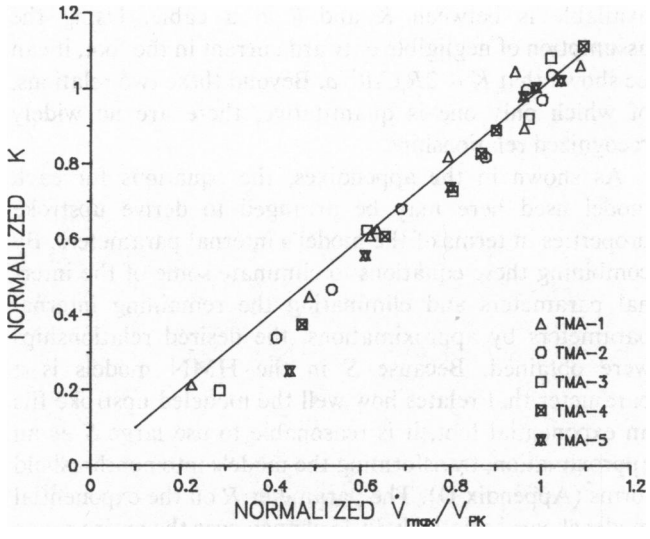

FIGURE 9 Comparison of K values, normalized to control, with normalized V_{max}/V_{pk} values. Straight line is ideal line for $K \propto V_{max}/V_{pk}$. Different symbols for individual experiments.

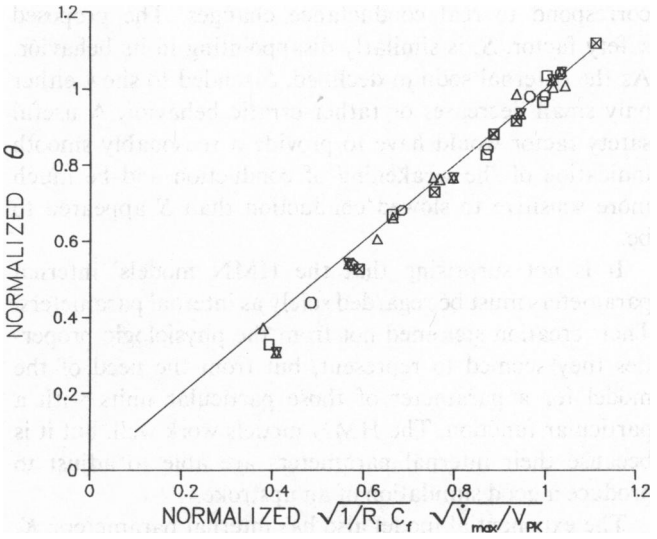

FIGURE 11 Comparison of normalized θ and $\dot{V}_{max}$ using model derived relationship (line). Different symbols for different experiments.

cally more reasonable. However, for an exponential rise of the action-potential foot to occur, the ionic current during the foot must be zero. From experimental studies, peak inward current is around 2,000 $\mu A/cm^2$. This is compared with a negligible outward current of perhaps 30 $\mu A/cm^2$. In this way, when scaled to the peak currents, the presence or absence of a threshold makes little difference because the actual outward current that occurs is indistinguishable from zero.

The models all have internal parameters. The internal parameters of the HMN models were originally presented as possibly having physiologic significance; i.e., V_{th} is threshold potential, S is safety factor, and G is related to sodium conductance. In the results obtained here, it was seen that they did not respond as expected of the physiological variables. V_{th} either showed relatively little change or tended to decrease as external sodium decreased, whereas V_{th} would be expected to rise with decreasing sodium current.

A similar argument can be made against the rise in the G parameter observed here being a representation of actual conductance changes. Even with greater time-dependent activation due to the slower rise in potential, the decreased external sodium obviously dominates, because conduction slows. A constant or increased G obviously does not

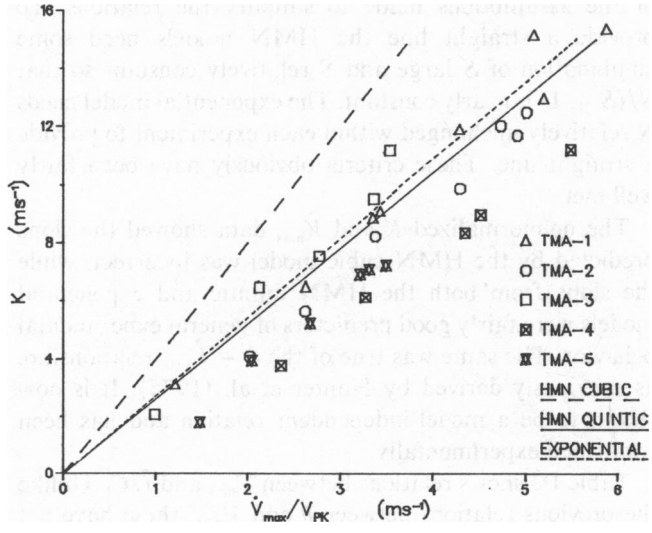

FIGURE 10 Comparison of data values of K and $\dot{V}_{max}/V_{pk}$ of lowered Na experiments. Also shown are lines of $K \propto V_{max}/V_{pk}$ predicted by models when assumptions of S large or R constant (=1) are applied. Different symbols for individual experiments.

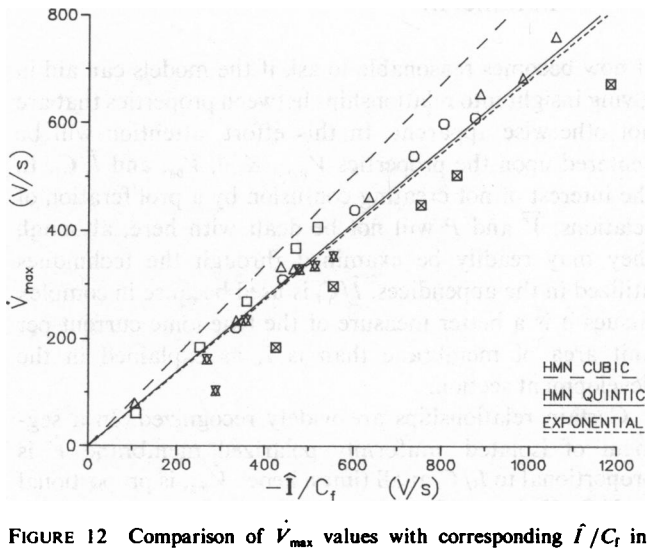

FIGURE 12 Comparison of $\dot{V}_{max}$ values with corresponding $\hat{I}/C_f$ in experiments of lowered Na. Lines are for predictions of HMN models with simplification of using S large and for exponential model with assumption of constant $R = 1$. Different symbols for individual experiments.

correspond to real conductance changes. The proposed safety factor, S, is similarly disappointing in its behavior. As the external sodium declined, S tended to show either only small decreases or rather erratic behavior. A useful safety factor would have to provide a reasonably smooth indication of the weakening of conduction and be much more sensitive to slowed conduction than S appeared to be.

It is not surprising that the HMN models' internal parameters must be regarded solely as internal parameters. Their creation stemmed not from the physiologic properties they seemed to represent, but from the need of the model for a parameter of those particular units with a particular function. The HMN models work well, but it is because their internal parameters are able to adjust to produce a good simulation of an upstroke.

The exponential model also has internal parameters: K, α, and β. K clearly is made equivalent to the physiologic rate constant of the foot, and it works well for this purpose. The parameter α is little more than a scaling factor that helps to set the starting level of the decline in $\dot{V}$. The ability to set it constant over all upstrokes in a fiber and still get good results with the model also indicates that it has little physiologic meaning. β is responsible, in part, for the rate of decrease in $\dot{V}$. Its overall significance was discussed when the model was presented, where β was qualitatively related to the overall rate of decline in inward current, and should be at least partially related to K. This was seen in the results section (Figs. 7 and 8), where β slowed similar to the decline in K and the ratio $K/\beta = R$ was maintained quite well considering the large changes in conduction that occurred.

Relationships Between the Upstroke Parameters

It now becomes reasonable to ask if the models can aid in giving insight into relationships between properties that are not otherwise apparent. In this effort, attention will be centered upon the properties $\dot{V}_{max}$, K, θ, V_{pk}, and $\hat{I}/C_f$. In the interest of not creating confusion by a proliferation of relations, $\overline{V}$ and P will not be dealt with here, although they may readily be examined through the techniques utilized in the appendices. $\hat{I}/C_f$ is used because in complex tissues it is a better measure of the true ionic current per unit area of membrane than is $\hat{I}$, as explained in the development section.

Certain relationships are widely recognized. In a segment of isolated, uniformly polarized membrane $\dot{V}$ is proportional to I_i/C_f at all times, hence $\dot{V}_{max}$ is proportional to $\hat{I}/C_f$. However, for a propagating action potential, the relationship is much more complex. Although it is widely accepted that if $\hat{I}/C_f$ increases, then $\dot{V}_{max}$ will increase, it is not at all clear what, if any, quantitative relationship occurs between them. The only quantitative relationship available is between K and θ in a cable. Using the assumption of negligible outward current in the foot, it can be shown that $K = 2R_iC_f\theta^2/a$. Beyond these two relations, of which only one is quantitative, there are no widely recognized relationships.

As shown in the appendixes, the equations for each model used here may be arranged to derive upstroke properties in terms of the model's internal parameters. By combining these equations to eliminate some of the internal parameters and eliminating the remaining internal parameters by approximations, the desired relationships were obtained. Because S in the HMN models is a parameter that relates how well the modeled upstroke fits an exponential foot, it is reasonable to use large S as an approximation, transforming the models into nonthreshold forms (Appendix D). The parameter R on the exponential model showed relatively little change over the entire range of conduction seen here. In particular, $R = 1$ was about the midrange of R values obtained when the individual upstrokes were modeled, and makes a convenient choice to use when a specific R is needed.

For the relations between K and $\dot{V}_{max}$ (Table II), it was apparent that the simplified relations were identical except for slope. Because the models have considerably different basic forms, this implies that their differences are unimportant. The results are produced from that part of their basis that is common—the cable equation. Stated differently, the relations are not artifacts of the particular forms chosen to model the upstroke, but are simply a consequence of uniform conduction in a cable.

The relationships also clearly fit the experimental data well. This also serves to confirm the judgement that the relationships are a result of the conditions of propagation, not of the details of the form of the model's equation. The closeness to the straight line fit also is a partial verification of the assumptions made to simplify the relations. To provide a straight line the HMN models need some combination of S large and S relatively constant so that $S/(S + 1)$ is nearly constant. The exponential model needs R relatively unchanged within each experiment to provide a straight line. These criteria obviously have been fairly well met.

The nonnormalized K and $\dot{V}_{max}$ data showed the slope predicted by the HMN cubic model was incorrect, while the slope from both the HMN quintic and exponential models were fairly good predictors of general experimental behavior. The same was true of the $\theta - \dot{V}_{max}$ relationship, as previously derived by Hunter et al. (1975). It is now shown to be a model-independent relation and has been confirmed experimentally.

Table III shows relations between $\dot{V}_{max}$ and $\hat{I}/C_f$. Unlike the previous relations between θ and $\dot{V}_{max}$, these have not been presented elsewhere before. Again, the agreement of all three models argues in favor of the cable relations being their source. This relation was also seen by Jenerick (1964) in his work with frog skeletal muscle, and was confirmed

by the data used here. The nonnormalized data showed the same behavior as did the relations. The cubic model's slope was inaccurate, but the quintic and exponential models gave slopes fairly similar to the experimental behavior.

The data for the remaining relations, between K or θ and $\hat{I}/C_f$ (Table IV) were not shown because they are just recombinations of the previously considered model and experimental relations. Because they are presented here for the first time, they are of interest in showing how θ (and K) is dependent upon $\hat{I}/C_f$. The arguments previously made in favor of the relation being a consequence of conduction in a cable are applicable here.

Also of interest at this point is a modeling method proposed by Matsumoto and Tasaki (1977). Their model uses a different development procedure than the models here used, but it too starts with a $\dot{V}$ curve. They depict their curve as a trapezoid. Hence their $V(t)$ curve has three segments: an exponential foot, a linear rise in potential ($\dot{V}$ is level), followed by an exponential decay to V_{pk}. By additionally postulating a constant membrane conductance in the third region, their result was an equation relating θ to the active membrane conductance. If this conductance is rewritten in terms of their peak current as ($\hat{I}/C_f$) and substituted into their equation for θ, the result differs from the relation between θ and $\hat{I}/C_f$ of Table IV only by a factor that may be written as $\sqrt{f/(f-1)}$ where f is somewhat analogous to S. Then the approximation of f large gives the same equation as obtained here. This is another example of a different model producing the same relation.

While these equations explain how the upstroke properties are related to each other, they do not offer any insight into the relationship between the upstroke properties and the basic membrane properties, such as single Na channel behavior. To examine these relationships, a model that explicitly deals with processes on that level must be used. Models of that level could then be joined with models of the sort used here to relate the I_i predicted to the upstroke properties.

Hunter et al. (1975) also developed models to deal with these membrane processes, which they called activation models. These can be combined with their HMN polynominal models used here to relate upstroke properties to basic membrane properties, particularly the ionic current channel's properties. Since the basic membrane processes are not readily subject to experimental manipulation, the models cannot be easily tested. In lieu of this, demonstration of the model independence of the resulting relations could provide a basis for confidence in them. However, the activation models have serious difficulties. A different membrane model had to be coupled to each of the HMN upstroke models, and the final relations produced were not the same, that is, not model independent. This is certain evidence of their containing model-introduced artifact. In light of this, their quantitative relationships must be regarded with caution.

The Problem of Safety Factor

The concept of safety factor has long been familiar to physiologists. While qualitatively well understood, it has been very difficult to measure. In Rushton's (1937) model V_{pk} served as both an internal parameter and an upstroke property, as it does in the HMN models. Rushton defined safety factor as $(V_{pk}/V_{pk,min}) - 1$ where $V_{pk,min}$ is the V_{pk} at which θ just falls to zero. Although his model is not directly applicable, his definition of safety factor is similar to that used for the HMN models. The S parameter was presented in the HMN models as being an actual safety factor, but we have demonstrated severe problems with accepting it as a good definition of safety factor. The geometric ratio (Goldstein and Rall, 1974) seems to give a quantitative measure of the change in safety factor for the specific condition of axon branching.

As a first step to finding a safety factor, criteria can be proposed that at least qualitatively describe its behavior and properties, but are independent of any model. A valid safety factor should be able to be evaluated by models of differing form. Another, intuitive concept of safety factor is that it should be dimensionless and directly reflect the underlying changes that cause the slowing of conduction. Finally, to be useful it should be possible, probably through the use of models of the types seen here, to determine the relationship of the upstroke parameters to the safety factor.

Power, or rate of energy change, seems a reasonable property to be included in a safety factor. If the electrical energy of a stimulus is applied slowly, the applied charge can redistribute along a long section of the cable, dissipating its effect and allowing accommodation. However, if too small a stimulus is applied from one segment to the next, propagation will fail, no matter how fast that stimulus is applied. As a measure of the stimulus size, the upstroke's

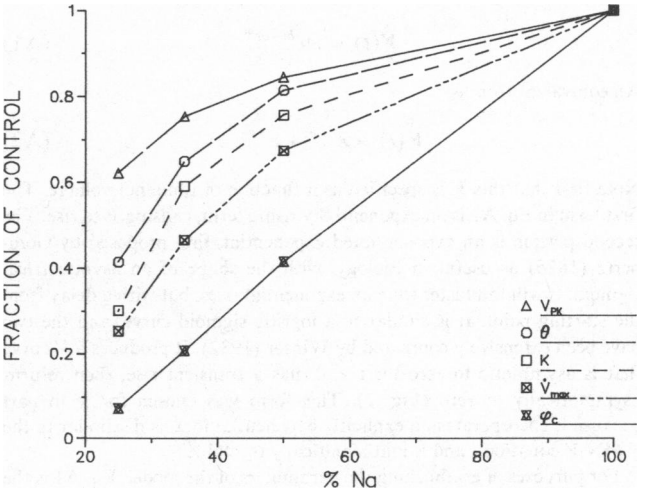

FIGURE 13 Values of ϕ_c ($-P_c U_c/C_f^2$) in lowered Na solutions. Points are average of normalized to control values at each Na level. Curves for V_{pk}, θ, K, $\dot{V}_{max}$ shown for comparison.

electrical energy change would seem useful. An intriguing result occurred when power and energy were combined in the manner of a simple product. The energy transferred into the membrane capacitance ($U_c = \int I_c V dt$) and the power of that transfer ($P_c = \int I_c dv$) were utilized. They have the same problems as $\hat{I}$, so that U_c/C_f and P_c/C_f are valid for all tissues, and are likely to be more valid for the cardiac Purkinje fibers used here. $(P_c/C_f) \cdot (U_c/C_f)$, which will be referred to as ϕ_c, is not a unitless quantity, so cannot be readily compared between different fibers. Nonetheless, ϕ_c is at least independent of any single model's structure, and does turn out to have interesting behavior.

ϕ_c was calculated for the data, normalized for each fiber and averaged as the other properties, and is shown in Fig. 13. It is readily seen that ϕ_c is nearly linear as the percentage of Na declines. ϕ_c is also very near zero for the last action potentials that were conducted, and extrapolation would put it at zero for the next step of lowered sodium. The best approximation of the underlying change is a decrease in sodium conductance as external sodium declines, and may be roughly linear with the sodium level. Hence, ϕ_c seems as though it may roughly linearly reflect the change in conductance.

The ϕ_c parameter is certainly not a true safety factor, but it does seem to have certain useful attributes that were lacking in the HMN model's S parameter. It may be a useful step in the development of a complete description of the balance between the active and the passive properties that determine conduction.

APPENDIX A

Exponential Model

Development of the Model. A relative membrane potential will be used, where resting potential is defined as zero, and the height of the upstroke is a positive potential V_{pk}. The model begins with the postulate that the $\dot{V}(t)$ curve can be well modeled by the form

$$\dot{V}(t) = Ae^{bt - \alpha e^{\beta t}} \tag{A1}$$

An equivalent form is

$$\dot{V}(t) = e^{a+bt} \cdot e^{-e^{\beta t}}. \tag{A2}$$

Note first that this $\dot{V}$ is specified as a function of time, not voltage. The first term in Eq. A2 is an exponentially rising term, causing $\dot{V}$ to rise. The second portion is an exponentiated exponential, first proposed by Gompertz (1825) as useful in Biology, with the shape of an asymmetrical sigmoid. It will fall faster than an exponential rises, but with a delay from the starting point. It is similar to a logistic sigmoid curve, and the two have been extensively compared by Winsor (1932). It produces a $\dot{V}$ curve that is asymptotic to zero for $t < 0$, has a transient rise, then returns asymptotically to zero (Fig. 2). This form was chosen for $\dot{V}$ in part because it encorporates an explicitly exponential foot, is dissimilar to the HMN $\dot{V}$ equations, and is mathematically tractable.

For purposes of establishing the parameters of the model, Eq. A1 is the form that will be used, with A in V/s, b and β in s^{-1}, and α without units. To clarify these parameters somewhat, consider the early portion of an upstroke with an exponential foot: $V \sim C_1 e^{Kt}$, $\dot{V} \sim C_1 K e^{Kt}$, $\ln \dot{V} \sim \ln (C_1 K) + Kt$, all for t early. But the model predicts

$$\ln \dot{V} = \ln A + bt - \alpha e^{\beta t},$$

so that

$$\ln A + bt - \alpha e^{\beta t} \simeq \ln (C_1 K) + Kt.$$

Equating powers of t, $A \sim C_1 K$; $b \sim K$; and $\alpha e^{\beta t} \sim 0$. First note that A is just a scaled C_1, which only serves to set the starting point ($t = 0$) on the curve. For convenience, let $A = 1$ V/s. This makes $\dot{V}(0) = 1$ V/s, which is sufficiently early for upstrokes of the sort seen here that $t < 0$ may be ignored. The parameter B must be equal to K or else the foot of the model cannot match the experimental results of exponential rise with rate constant K. The last approximation can be true only if α is very small so that for small t the term is negligible.

The $\dot{V}$ equation with the above changes is

$$\dot{V}(t) = e^{Kt - \alpha e^{\beta t}} \tag{A3}$$

The cable equation with uniform conduction (Eq. 2) is used:

$$I_i = C_f(\ddot{V}/K - \dot{V}). \tag{2}$$

Now

$$\ddot{V} = \frac{d\dot{V}}{dt} = (K - \alpha\beta e^{\beta t})\, e^{Kt - \alpha e^{\beta t}}. \tag{A4}$$

Then

$$I_i = \frac{C_f}{K}(K - \alpha\beta e^{\beta t}) e^{Kt - \alpha e^{\beta t}} - C_f e^{Kt - \alpha e^{\beta t}}$$

$$I_i = -C_f \frac{\alpha\beta}{K} e^{\beta t} e^{Kt - \alpha e^{\beta t}} \tag{A5}$$

or

$$I_i = -\, C_f\, (\alpha\beta/K)\, e^{\beta t}\, \dot{V}.$$

Testing the model. $\dot{V}_{max}$ occurs at time $\bar{t}$, at which $\ddot{V} = 0$. From Eq. A4

$$\ddot{V}(\bar{t}) = 0 = (K - \alpha\beta e^{\beta \bar{t}})\, \dot{V}_{max}$$

$$\therefore K - \alpha\beta e^{\beta \bar{t}} = 0$$

$$\bar{t} = (1/\beta) \ln (K/\alpha\beta) = \ln (K/\alpha\beta)^{1/\beta}$$

$$\dot{V}_{max} = \dot{V}(\bar{t}) \tag{A6}$$

yielding

$$\dot{V}_{max} = \alpha^{-K/\beta}\, (K/\beta)^{K/\beta}\, e^{-K/\beta}. \tag{A7}$$

V_{pk} must be calculated.

$$V(t) = \int_{-\infty}^{t} \dot{V}\, dt \sim \int_{0}^{t} \dot{V}\, dt$$

because A was chosen small so that no significant amount occurred for $t < 0$:

$$V(t) = \int_0^t e^{Kt - \alpha e^{\beta t}}\, dt.$$

Using the substitution $z = \alpha e^{\beta t}$ produces

$$V(t) = \int_{\alpha}^{Z(t)} \alpha^{-K/\beta} Z^{K/\beta} e^{-Z} \frac{1}{\beta} Z^{-1}\, dz$$

$$V(t) = \alpha^{-K/\beta}\beta^{-1} \int_{\alpha}^{Z(t)} Z^{(K/\beta)-1} e^{-Z}\, dz.$$

But

$$\Gamma(x) \equiv \int_0^{\infty} z^{x-1} e^{-z} dz$$

$$\gamma(x,w) \equiv \int_0^{w} z^{x-1} e^{-z} dz.$$

$\Gamma(x)$ is the gamma function, a continuous analogue of the factorial function. $\gamma(x,w)$ is called the incomplete gamma function.

$$\therefore V(t) = \alpha^{-K/\beta}\beta^{-1}\left\{\gamma\left[\frac{K}{\beta}, z(t)\right] - \gamma\left(\frac{K}{\beta}, \alpha\right)\right\}. \quad \text{(A8)}$$

To find V_{pk}, use $t \rightarrow \infty$

$$z(t) \rightarrow \alpha e^{\beta\infty} \rightarrow \infty$$

$$\gamma(x, \infty) = \Gamma(x)$$

$$V_{pk} = \alpha^{-K/\beta}\beta^{-1}[\Gamma(K/\beta) - \gamma(K/\beta, \alpha)].$$

If α is very small, and $K/\beta = R$, which is neither very big nor very small, then

$$\gamma(R\,\alpha) \approx 0$$

$$\therefore V_{pk} = \alpha^{-R}\beta^{-1}\Gamma(R). \quad \text{(A9)}$$

Now find $\hat{I}$, which occurs at $\hat{t}$. From Eq. A5

$$\dot{I}_i = C_f(\alpha\beta/K)e^{\beta t}\dot{V}(\beta + K - \alpha\beta e^{\beta t}).$$

At $\hat{t}$

$$\dot{I}_i = 0 \qquad \text{But } \dot{V} \neq 0$$

$$\therefore \beta + K - \alpha\beta e^{\beta \hat{t}} = 0$$

and

$$\hat{t} = (1/\beta)\ln\left(\frac{K+\beta}{\alpha\beta}\right). \quad \text{(A10)}$$

Inserting $R = K/\beta$ into Eq. 5 gives

$$\hat{I} = -\alpha^{-R} C_f R^{-1}\left(\frac{R+1}{e}\right)^{R+1}. \quad \text{(A11)}$$

Also derive an equation for power,

$$P = \int_0^{V_{pk}} I_i dV = \int_0^{V_{pk}} -C_f\frac{\alpha\beta}{K}e^{\beta t}\dot{V}\, dV$$

$$= -\frac{C_f\alpha\beta}{K}\int_0^{\infty} e^{\beta t} e^{2Kt} e^{-2\alpha e^{\beta t}} dt.$$

Similar to the process for V_{pk}, use $z = 2\alpha e^{\beta t}$ resulting in

$$P = -\alpha^{-2R} 2^{-(2R+1)}(C_f/K)\Gamma(2R+1),$$

but $x\Gamma(x) = \Gamma(x+1)$

$$\therefore P = -\alpha^{-2R} 2^{-2R}\frac{C_f}{\beta}\Gamma(2R). \quad \text{(A12)}$$

To apply the model using K, $\dot{V}_{max}$, and V_{pk} as input data, combine Eqs. A7 and A9 to eliminate α^{-R}:

$$\dot{V}_{max} = \frac{V_{pk}\beta}{\Gamma(R)}(R/e)^R.$$

$$\therefore \dot{V}_{max} - \frac{V_{pk}\beta}{\Gamma(R)}(R/e)^R = 0 \quad \text{(A13)}$$

is a function of β only since $\dot{V}_{max}$, V_{pk} and K are known. Search for values of β that solve the equation, then

$$\alpha = \left(\frac{V_{pk}\beta}{\Gamma(R)}\right)^{-(1/R)}$$

and the model is solved.

When using $\hat{I}$ as input, choose an α that is constant to provide the third constraint. Eq. A11 is an equation in one variable, R. Find the R giving solution, then use Eq. A12 to find β, and calculate $K = R \cdot \beta$.

Relations between Upstroke Parameters. Using Eq. A13 and $K = R\beta$

$$\dot{V}_{max} = V_{pK}KR^{-1}\Gamma(R)^{-1}R^R e^{-R}$$

$$K = \frac{e^R}{R^{R-1}}\Gamma(R)\frac{\dot{V}_{max}}{V_{pk}}. \quad \text{(A14)}$$

Converting to θ with Eq. 4

$$\theta = \sqrt{\frac{e^R}{2R^{R-1}}}\Gamma(R)\sqrt{\frac{a}{R_i C_f}}\sqrt{\frac{\dot{V}_{max}}{V_{pk}}}. \quad \text{(A15)}$$

Combining $\hat{I}$ and V_{pk}

$$\hat{I}/C_f = -R^{-2}K\Gamma(R)^{-1}\left(\frac{R+1}{e}\right)^{R+1}V_{pk}$$

$$K = -R^{-2}\left(\frac{e}{R+1}\right)^{R+1}\Gamma(R)\frac{\hat{I}/C_f}{V_{pK}} \quad \text{(A16)}$$

$$\theta = \sqrt{R^2\left(\frac{e}{R+1}\right)^{R+1}\Gamma(R)}\sqrt{\frac{a}{2R_i C_f}}\sqrt{\frac{-\hat{I}/C_f}{V_{pk}}} \quad \text{(A17)}$$

Combining $\hat{I}$ and $\dot{V}_{max}$,

$$\dot{V}_{max} = e\left(\frac{R}{R+1}\right)^{R+1}\hat{I}/C_f. \quad \text{(A18)}$$

APPENDIX B

HMN Cubic Model

The following development of the HMN cubic model is modified from that presented by Hunter et al. (1975) only in the method of development. Parameters of the model are converted at the end into those used in the original article, and thereafter only those are dealt with. The purpose of the modified development is, first, that all the models use the same method of development. In that way, it becomes easier to see the

similarities and differences between the models. Second, it becomes clearer both where in the models a priori postulates are introduced and what significance the associated parameters have.

Development of Basic Model. This model is developed in much the same way as the exponential model; here we postulate that the $\dot{V}(V)$ curve can be well modeled by a parabola (Fig. 1 *B*) whose form is

$$\dot{V} = MV(1 - V/V_{pk}). \tag{B1}$$

This curve is zero at $V = 0$, rises to a peak ($\dot{V}_{max}$) at some particular potential ($\bar{V}$) and then declines to zero at V_{pk}. The initial slope (at $V = 0$) is M, with units of $1/t$. The model can now be developed in the same way as previous models. Apply the cable relation, Eq. 2:

$$I_i = C_f(\ddot{V}/K - \dot{V}) \tag{2}$$

$$\ddot{V} = \frac{d\dot{V}}{dt} = \frac{d\dot{V}}{dV}\cdot\frac{dV}{dt} = \dot{V}\frac{d\dot{V}}{dV}$$

$$\therefore \ddot{V} = \dot{V}\frac{d}{dV}\left[MV\left(1 - \frac{V}{V_{pk}}\right)\right]$$

$$\ddot{V} = \dot{V}M\left[1 - \frac{V}{V_{pk}} - \frac{V}{V_{pk}}\right] = M\dot{V}\left(1 - \frac{2V}{V_{pk}}\right) \tag{B2}$$

$$\therefore I_i = C_f\left[M\dot{V}\left(1 - \frac{2V}{V_{pk}}\right)\Big/K - \dot{V}\right]. \tag{B3}$$

This I_i curve, called the current trajectory, is a cubic function of V. It has three roots, at $V = 0$, $V = V_{pk}$ and $(2/V_{pk})V = 1 - K/M$. Because both V and $1 - (V/V_{pk})$ are always positive, the third term controls the current's polarity. Now the second a priori postulate is made, that the I_i trajectory exhibits a threshold phenomenon (Fig. 1 *C*). This means that for early portions of the upstroke, I_i is outward. At some potential (V_{th}) it changes to inward current (negative) as the Na current begins to dominate. Its value increases to some negative peak value ($\hat{I}$) and then falls to zero at V_{pk}. If $K/M > 1$, then $1 - (K/M) < 0$ and I_i is always inward. For a threshold I_i, $K/M < 1$ is required. To ensure this occurs, use a new parameter S, where $S \in (0,\infty)$ and is unitless. Set

$$K/M = S/(S + 1), \tag{B4}$$

which is always positive and <1. Then

$$I_i = \frac{C_f M^2}{K} V\left(1 - \frac{S}{S+1} - \frac{2}{V_{pk}}V\right)\left(1 - \frac{V}{V_{pk}}\right). \tag{B5}$$

To simplify, use the forced middle root, V_{th}. Its value may be found by using the fact that, at V_{th}

$$1 - \frac{S}{S+1} - 2\frac{V_{th}}{V_{pk}} = 0 \tag{B6}$$

$$V_{th} = \frac{V_{pk}}{2}\left(\frac{1}{S+1}\right). \tag{B7}$$

Hence, the parameter S, introduced to ensure a threshold phenomenon, acts to set the value of V_{th}. Alternatively V_{th} and V_{pk} set S

$$S = \frac{1}{2}\frac{V_{pk}}{V_{th}} - 1 \tag{B8}$$

Note how requirement of $S > 0$ means $V_{th} < V_{pk}/2$. Then, using Eqs. B4 and B5

$$I_i = \frac{C_f M}{S} V\left(1 - \frac{V}{V_{th}}\right)\left(1 - \frac{V}{V_{pk}}\right). \tag{B9}$$

$C_f M/S$ has units of farads per area-seconds, which is conductance per unit area. Therefore, replace $C_f M/S$ by a new parameter G with units of conductance per unit area.

$$I_i = GV\left(1 - \frac{V}{V_{th}}\right)\left(1 - \frac{V}{V_{pk}}\right). \tag{B10}$$

It is apparent from the definition of K used here that it is actually the same as K of Eq. 4, which was the rate constant of the experimental upstrokes' exponential foot. The parameter M is the model's analogue of the rate constant. In other words, $M/K = 1 + 1/S$ is a measure of how well the model reproduces an exponential foot. When $M/K \sim 1$ (or $S \to \infty$), the modeled early foot is approximately exponential. Then S may be interpreted as a parameter indicating how close the modeled foot is to being exponential. However, to prevent any confusion between two rate constants when using the model, replace M by its equivalent in G, $M = GS/C_f$:

$$\dot{V}(V) = \frac{GS}{C_f} V\left(1 - \frac{V}{V_{pk}}\right). \tag{B11}$$

Solely from definitions, K may also be rewritten:

$$K = \frac{GS}{C_f}\left(\frac{S}{S+1}\right). \tag{B12}$$

This is a three-parameter model, V_{pk}, V_{th}, and G. S is related to V_{pk} and V_{th}. C_f is just a parameter of the particular cable being modeled.

Testing of the Model. The model is applied through use of data values for V_{pk}, K, $\dot{V}_{max}$, $\hat{I}$ and P. V_{pk} is an intrinsic parameter. For $\dot{V}_{max}$ from Eq. B11

$$\frac{d\dot{V}}{dV} = \frac{GS}{C_f}\left(1 - \frac{2V}{V_{pk}}\right)$$

$d\dot{V}/dV = 0$ at $\dot{V}_{max}$, when $V = \bar{V}$

$$\frac{GS}{C_f}\left(1 - \frac{2\bar{V}}{V_{pk}}\right) = 0$$

$$\therefore \bar{V} = \frac{V_{pk}}{2}$$

$$\therefore \dot{V}_{max} = \dot{V}(\bar{V}) = (1/4)\frac{GS}{C_f}V_{pk}. \tag{B13}$$

Similarly, peak inward current $\hat{I}$ may be found by finding $\hat{V}$ from Eq. A10

$$\frac{dI_i}{dV} = G\left[\left(1 - \frac{2V}{V_{th}}\right)\left(1 - \frac{V}{V_{pk}}\right) - \frac{V}{V_{pk}}\left(1 - \frac{V}{V_{th}}\right)\right]$$

at $\hat{V}$, $dI_i/dV = 0$

$$\therefore \left(1 - \frac{2\hat{V}}{V_{th}}\right)\left(1 - \frac{\hat{V}}{V_{pk}}\right) - \frac{\hat{V}}{V_{pk}}\left(1 - \frac{\hat{V}}{V_{th}}\right) = 0$$

$$\hat{V} = \frac{2(V_{th} + V_{pk}) \pm \sqrt{4V_{th}^2 + 8V_{th}V_{pk} + 4V_{pk}^2 - 12V_{th}V_{pk}}}{6}.$$

For $\hat{I}$, use the positive square root to give the second peak, the first being the outward peak.

$$\hat{V} = (1/3)\left(V_{th} + V_{pk} + \sqrt{V_{th}^2 - V_{th}V_{pk} + V_{pk}^2}\right) \tag{B14}$$

$\hat{I}$ may then be found by inserting $\hat{V}$ in Eq. B10. Last, calculate the power to the peak of the upstroke:

$$P = \int_0^{V_{pk}} I_i \, dV$$

$$= G\left[\frac{1}{2}V^2 - \frac{1}{3}\left(\frac{1}{V_{th}} + \frac{1}{V_{pk}}\right)V^3 + \frac{1}{4V_{th}V_{pk}}V^4\right]_0^{V_{pk}}$$

$$P = \frac{-GV_{pk}^2 S}{6}. \tag{B15}$$

Using the velocity related data, G, V_{th}, V_{pk} must be set, given $\dot{V}_{max}$, V_{pk}, and K. V_{pk} of the data is used directly as the model's V_{pk}. Then, substituting into Eq. B13, Eq. B12 eliminates GS/C_f, and Eq. B8 eliminates S, resulting in a solution for V_{th}:

$$V_{th} = \frac{1}{2}V_{pk} - \frac{1}{8}\frac{KV_{pk}^2}{\dot{V}_{max}}.$$

Then, with Eq. B8 and B12, V_{pk}, V_{th}, G, and S are obtained from $\dot{V}_{max}$, V_{pk}, and K.

Only two current related parameters are available, $\hat{I}$, P. To provide the third constraint necessary to solve for the model's parameters, several methods are available. First, one of the model's parameters may be given a value leaving only two free parameters. The G value might be made constant for all upstrokes in each fiber, or it might decline, approximately with the percent of Na, due to the effective decline of the Na conductance as Na decreased. Holding V_{th} constant in each fiber was also utilized as a third, simply implemented method of fixing a parameter. A fourth method was to set the last parameter, V_{pk} by utilizing the actual data value.

For the constant G method, G was set to a value about the midrange of those obtained above for each fiber. Then, using $r = V_{th}/V_{pk}$ as a temporary variable,

$$P = \frac{-GV_{pk}^2}{6}\left(\frac{1}{2r} - 1\right)$$

$$\therefore V_{pk}^2 = \frac{6P}{G(1 - 1/2r)} = \frac{6P}{G}\left(\frac{2r}{2r - 1}\right)$$

$$V_{pk} = \sqrt{\frac{6P}{G}\left(\frac{2r}{2r - 1}\right)}$$

and $V_{th} = r \cdot V_{pk}$, so that

$$\hat{V}(r) = (1/3)\left(V_{pk} + V_{th} + \sqrt{V_{pk}^2 - V_{pk}V_{th} + V_{th}^2}\right)$$

may be calculated and

$$\hat{I}(r) = I_i[\hat{V}(r)].$$

Then, for a solution, test

$$I_r[\hat{V}(r)] - \hat{I}_{data} = 0.$$

Therefore, search through $r \in (0, \frac{1}{2})$ for value(s), solve the equation, and, using that r, calculate solution values V_{pk} and V_{th}.

For the decreasing G method, a G value was chosen for the 100% Na upstrokes, and G was forced to vary proportionally with the percent Na. For the constant V_{th} method, a V_{th} value was chosen for each fiber from about the midrange of the V_{th} values obtained above. Then a tentative V_{pk} value was chosen, and using Eq. B8 and B15, a $\hat{V}(V_{pk})$ was evaluated. The equation

$$I_i[\hat{V}(V_{pk})] - \hat{I}_{data} = 0$$

was tested for a solution. Values of V_{pk} were searched for a solution, and G and S calculated from the final V_{pk}. Finally, the actual data value for V_{pk} was utilized with $\hat{I}$ and P. In a manner similar to the above method, a tentative choice of V_{th} and Eqs. B8 and B15 allow calculation of $\hat{V}(V_{th})$ and testing $I_i[\hat{V}(V_{th})] - \hat{I}_{data} = 0$. Values of V_{th} were searched on $V_{th} \in (0, V_{pk}/2)$ for solutions, and final values of S and G were calculated.

Relations between Upstroke Parameters. Previously derived equations are

$$S = \frac{V_{pk}}{2V_{th}} - 1 \tag{B8}$$

$$K = \frac{GS}{C_f}\left(\frac{S}{S + 1}\right) \tag{B12}$$

$$\dot{V}_{max} = \frac{GS\,V_{pk}}{4C_f} \tag{B13}$$

$$P = \frac{-G\,V_{pk}^2}{6}S \tag{B15}$$

$$\hat{V} = (1/3)(V_{th} + V_{pk} + \sqrt{V_{ph}^2 - V_{th}V_{pk} + V_{pk}^2}). \tag{B14}$$

This may be rewritten in terms of S, and then substituted into $I_i(V)$ for $\hat{I}$. Purely routine algebraic steps with no simplifying assumptions lead to an equation for $\hat{I}$

$$\hat{I} = \frac{1}{54}\frac{G\,V_{pk}}{(S + 1)^2}$$

$$\cdot [9S + 18S^2 - 8S^3 - (2S + 1)^2\sqrt{4S^2 + 10S + 7}] \tag{B16}$$

But if S is large,

$$\hat{I} = -\frac{8}{27}GV_{pk}S. \tag{B17}$$

These equations may be rearranged to show relations between the upstroke parameters. Using K, eliminate GS from $\dot{V}_{max}$ and $\hat{I}$:

$$K = \frac{4\dot{V}_{max}}{V_{pk}}\left(\frac{S}{S + 1}\right) \tag{B18}$$

$$\hat{I} = -\frac{8}{27}KC_f\left(\frac{S + 1}{S}\right)V_{pk}$$

$$K = -\frac{27}{8}\frac{\hat{I}/C_f}{V_{pk}} \quad \text{for large } S. \tag{B19}$$

Relating $\dot{V}_{max}$ to $\hat{I}/C_f$

$$\frac{4\dot{V}_{max}}{V_{pk}} = -\frac{27}{8}\frac{\hat{I}/C_f}{V_{pk}} \quad \text{for large } S \tag{B20}$$

$$\dot{V}_{max} = -\frac{27}{32}\hat{I}/C_f. \tag{B21}$$

Thus, $\hat{I}/C_f$ and $\dot{V}_{max}$ are linearly related for large S. To find relations for θ use the relations involving K,

$$K = \frac{2R_iC_f\theta^2}{a} = \frac{4\dot{V}_{max}}{V_{pk}}\left(\frac{S}{S + 1}\right)$$

$$\theta = \sqrt{\frac{2a}{R_iC_f}}\sqrt{\frac{\dot{V}_{max}}{V_{pk}}}\sqrt{\frac{S}{S + 1}} \tag{B22}$$

$$\theta = \sqrt{\frac{2a}{R_i C_f}}\sqrt{\frac{\dot{V}_{max}}{V_{pk}}} \quad \text{for large } S. \tag{B23}$$

Also, for $\hat{I}/C_f$ when S is large

$$K = \frac{2R_i C_f \theta^2}{a} = -\frac{27}{8}\frac{\hat{I}/C_f}{V_{pk}}$$

$$\theta = \sqrt{\frac{27a}{16R_i C_f}}\sqrt{\frac{-\hat{I}/C_f}{V_{pk}}}. \tag{B24}$$

P may also be related to the other parameters

$$P = -\frac{GSV_{pk}^2}{6}$$

For K

$$P = \frac{1}{6}K C_f V_{pk}^2\left(\frac{S+1}{S}\right).$$

$$= \frac{K C_f V_{pk}^2}{6} \quad \text{for large } S. \tag{B25}$$

For $\hat{I}$,

$$P = -\frac{1}{6}\left(-\frac{27}{8}\frac{\hat{I}/C_f}{V_{pk}}\right)C_f V_{pk}^2$$

$$P = \frac{9}{16}\hat{I}\,V_{pk} \quad \text{for large } S.$$

APPENDIX C

HMN Quintic Model

The development, application, and relations are obtained similarly to the manner for the cubic model.

Development of Model. Again, the first postulate is the form of $\dot{V}$

$$\dot{V}(V) = MV\left(1 - \frac{V^2}{V_{pk}^2}\right). \tag{C1}$$

This is a cubic $\dot{V}$ curve. It is a skewed analogue of the cubic model's $\dot{V}$ curve. The cable relation is again applied, $V\,d\dot{V}/dV$ substituted for $\ddot{V}$ giving

$$I_i = \frac{C_f M^2}{K}V\left(1 - \frac{K}{M} - \frac{3V^2}{V_{pk}^2}\right)\left(1 - \frac{V^2}{V_{pk}^2}\right). \tag{C2}$$

Again postulating an I_i trajectory showing a threshold, introduces $S \in (0, \infty)$

$$K/M = \frac{S}{S+1}$$

$$I_i = \frac{C_f M^2}{K}V\left(1 - \frac{S}{S+1} - \frac{3V^2}{V_{pk}^2}\right)\left(1 - \frac{V^2}{V_{pk}^2}\right).$$

Again V_{th} comes from the middle root

$$\frac{3V_{th}^2}{V_{pk}^2} = 1 - \frac{S}{S+1} = \frac{1}{S+1}$$

$$S = \frac{V_{pk}^2}{3V_{th}^2} - 1$$

$$I_i = \frac{C_f M}{S}V\left(1 - \frac{V^2}{V_{th}^2}\right)\left(1 - \frac{V^2}{V_{pk}^2}\right). \tag{C3}$$

Setting $G = C_f M/S$

$$I_i = GV\left(1 - \frac{V^2}{V_{th}^2}\right)\left(1 - \frac{V^2}{V_{pk}^2}\right). \tag{C4}$$

And

$$\dot{V}(V) = \frac{GS}{C_f}V\left(1 - \frac{V^2}{V_{pk}^2}\right) \tag{C5}$$

$$K = \frac{GS}{C_f}\left(\frac{S}{S+1}\right). \tag{C6}$$

This is again a three-parameter model, but with a quintic I_i trajectory.

Application of the Model. This is done just as for the cubic model. The necessary equations are derived in the same manner yielding

$$\bar{V} = \frac{1}{\sqrt{3}}V_{pk} \tag{C7}$$

$$\dot{V}_{max} = \frac{2}{3\sqrt{3}}\frac{GSV_{pk}}{C_f} \tag{C8}$$

$$\hat{V} = \sqrt{\frac{3(V_{th}^2 + V_{pk}^2) + \sqrt{9V_{th}^4 - 2V_{th}^2V_{pk}^2 + 9V_{pk}^4}}{10}} \tag{C9}$$

$$\hat{I} = I_i(\hat{V})$$

$$P = -\frac{GSV_{pk}^2}{4}. \tag{C10}$$

Using $\dot{V}_{max}$, V_{pk}, K as input values

$$V_{th} = V_{pk}\sqrt{\frac{1}{3} - \frac{2KV_{pk}}{9\sqrt{3}\dot{V}_{max}}}$$

$$S = \frac{V_{pk}^2}{3V_{th}^2} - 1$$

$$G = \frac{3\sqrt{3}}{2}\frac{C_f\dot{V}_{max}}{V_{pk}S}.$$

The current-related parameters, $\hat{I}$ and P can be applied in the same way as for the cubic model. However, because the declining G method produced poor results in the cubic model, it was not used with the quintic model. For constant G, a value was chosen for each fiber from the midrange of the G values of each fiber produced above. Then, using a temporary variable $r = V_{th}/V_{pk}$,

$$S = \frac{1}{3r^2} - 1;\ V_{pk} = \sqrt{\frac{-4P}{GS}};\ V_{th} = r \cdot V_{pk}.$$

$\hat{V}(r)$ was calculated, $I_i[\hat{V}(r)] - \hat{I}_{data} = 0$ was tested, and $r \epsilon (0, 1/\sqrt{3})$ was searched for solutions, from which final values for V_{th}, V_{pk} could be calculated. For constant V_{th}, a value was chosen from about the midrange of each fiber's results above. With a tentative V_{pk} value,

$$S = \frac{V_{pk}^2}{3V_{th}^2} - 1 \; ; \; G = \frac{-4P}{V_{pk}^2 S}.$$

$\hat{V}(V_{pk})$ was calculated, and $I_i[\hat{V}(V_{pk})] - \hat{I}_{data} = 0$ tested for a solution, from which final values for V_{pk}, G could be calculated. Using $\hat{I}$, P, and V_{pk} as input values, with a tentative V_{th}, S is calculated from Eq. C3, G is calculated from Eq. C10, and $\hat{V}(V_{th})$ is calculated from Eq. C9, from which

$$I_i[\hat{V}(V_{th})] - \hat{I}_{data} = 0$$

is tested over $V_{th} \epsilon (0, V_{pk}/\sqrt{3})$ for solutions, from which final values of V_{th}, G were obtained.

Relations of Upstroke Parameters. As with the cubic, $\hat{I}$ may be explicitly derived. When the approximations for S large are made

$$\hat{I} = -\frac{18}{25}\sqrt{\frac{3}{5}}GSV_{pk}. \tag{C11}$$

As before, the equations developed above may be rearranged for relations between the upstroke parameters

$$K = \frac{3\sqrt{3}}{2}\frac{\dot{V}_{max}}{V_{pk}}\left(\frac{S}{S+1}\right) \tag{C12}$$

$$= \frac{3\sqrt{3}}{2}\frac{\dot{V}_{max}}{V_{pk}} \quad \text{for large } S \tag{C13}$$

$$K = -\frac{25}{18}\frac{\sqrt{5}}{3}\frac{\hat{I}/C_f}{V_{pk}} \quad \text{for large } S \tag{C14}$$

$$\dot{V}_{max} = -\frac{25}{81}\sqrt{5}\,\hat{I}/C_f \quad \text{for large } S \tag{C15}$$

$$\theta = \sqrt{\frac{3\sqrt{3}}{4}\frac{a}{R_i C_f}}\sqrt{\frac{\dot{V}_{max}}{V_{pk}}}\sqrt{\frac{S}{S+1}}$$

$$\theta = \sqrt{\frac{3\sqrt{3}}{4}\frac{a}{R_i C_f}}\sqrt{\frac{\dot{V}_{max}}{V_{pk}}} \quad \text{for large } S \tag{C16}$$

$$\theta = \sqrt{\frac{25\sqrt{15}}{108}\frac{a}{R_i C_f}}\sqrt{\frac{\hat{I}/C_f}{V_{pk}}} \quad \text{for large } S \tag{C17}$$

$$P = -\frac{C_f K V_{pk}^2}{4}\left(\frac{S+1}{S}\right)$$

$$P = \frac{25}{72}\frac{\sqrt{5}}{3}\hat{I}\,V_{pk} \quad \text{for large } S. \tag{C18}$$

APPENDIX D

HMN Nonthreshold Models

Models with polynomial forms for $\dot{V}$ and I_i may also be developed for nonthreshold I_i trajectories. They are developed in the same way as the cubic model, but no postulate of the presence or absence of a threshold is needed. The form chosen for $\dot{V}(V)$ automatically insures a nonthreshold I_i. Choosing

$$\dot{V} = KV\left(1 - \frac{V}{V_{pk}}\right)$$

leads to

$$I_i = -GV^2\left(1 - \frac{V}{V_{pk}}\right)$$

$$G = \frac{2KC_f}{V_{pk}}.$$

Note here that K is used as the slope of $\dot{V}$ for V small. This is the equivalent of letting $S \to \infty$ in the cubic model. This I_i is always negative, and is a cubic model nonthreshold current. The same sort of relations may be derived

$$K = 4\frac{\dot{V}_{max}}{V_{pk}} = -\frac{27}{8}\frac{\hat{I}/C_f}{V_{pk}}$$

$$\dot{V}_{max} = -\frac{27}{32}\hat{I}/C_f$$

$$\theta = \sqrt{\frac{2a}{R_i C_f}}\sqrt{\frac{\dot{V}_{max}}{V_{pk}}} = \sqrt{\frac{27a}{16R_i C_f}}\sqrt{\frac{-\hat{I}/C_f}{V_{pk}}}.$$

Note that these are the relations, including the same slopes, that the threshold cubic model produces when S large is assumed. A similar process will produce a quintic nonthreshold model.

This paper was supported by U.S. Public Health Service Grants HL-20592 and HD-07009.

Received for publication 22 June 1982 and in final form 5 May 1983.

REFERENCES

Cooley, J. W., and F. A. Dodge, Jr. 1966. Digital computer solutions for excitation and propagation of the nerve impulse. *Biophys. J.* 6:583–599.

Easton, D. M. 1978. Exponentiated exponential model (Gompertz kinetics) of Na^+ and K^+ conductance changes in squid giant axon. *Biophys. J.* 22:15-28.

FitzHugh, R. 1969. Mathematical models of excitation and propagation in nerve. *In* Biological Engineering. H.P. Schwan, editor. McGraw-Hill, Inc., New York. 1–85.

Goldstein, S. S., and W. Rall. 1974. Changes of action potential shape and velocity for changing core conductor geometry. *Biophys. J.* 14:731–757.

Gompertz, B. 1825. On the nature of the function expressive of the law of human mortality, and on a new method of determining the value of life contingencies. *Philos. Trans. Roy. Soc.* 513–585.

Hodgkin, A. L., and A. F. Huxley. 1952. A quantitative description of membrane current and its application to conduction and excitation in nerve. *J. Physiol. (Lond.)* 117:500–544.

Hunter, P. J., P. A. McNaughton and D. Noble. 1975. Analytical models of propagation in excitable cells. *Prog. Biophys. Mol. Biol.* 30:99–144.

Huxley, A. F. 1959. Ion movements during nerve activity. *Ann. NY Acad. Sci.* 81:221–246.

Jack, J. J. B., D. Noble, and R. W. Tsien. 1975. Electric Current Flow in Excitable Cells. Clarendon Press, Oxford, England. 282.

Jenerick, H. 1964. An analysis of the striated muscle fiber action current. *Biophys. J.* 4:77–91.

Khodorov, B. I., and E. N. Timin. 1975. Nerve impulse propagation along nonuniform fibers. *Prog. Biophys. Mol. Biol.* 30:145–184.

Levin, D. N., and H. A. Fozzard. 1981. A cleft model for cardiac Purkinje strands. *Biophys. J.* 33:383–408.

Matsumoto, G., and I. Tasaki. 1977. A study of conduction velocity in nonmyelinated nerve fibers. *Biophys. J.* 20:1–13.

Rushton, W. A. H. 1937. Initiation of the propagated disturbance. *Proc. R. Soc. Lond. B. Biol. Sci.* 124:210–243.

Tasaki, I., and S. Hagiwara. 1957. Capacity of muscle fiber membrane. *Am. J. Physiol.* 188:423–429.

Walton, M. K., and H. A. Fozzard. 1983. Experimental study of the conducted action potential in cardiac Purkinje strands. *Biophys. J.* 44:1–8.

Winsor, C. P. 1932. The Gompertz curve as a growth curve. *Proc. Natl. Acad. Sci. USA.* 18:1–18.